Apelin Inhibits Diet-Induced Obesity by Enhancing Lymphatic and Blood Vessel Integrity

Mika Sawane,[1,2] Kentaro Kajiya,[2] Hiroyasu Kidoya,[1] Masaya Takagi,[2] Fumitaka Muramatsu,[1] and Nobuyuki Takakura[1]

Angiogenesis is tightly associated with the outgrowth of adipose tissue, leading to obesity, which is a risk factor for type 2 diabetes and hypertension, mainly because expanding adipose tissue requires an increased nutrient supply from blood vessels. Therefore, induction of vessel abnormality by adipokines has been well-studied, whereas how altered vascular function promotes obesity is relatively unexplored. Also, surviving Prox1 heterozygous mice have shown abnormal lymphatic patterning and adult-onset obesity, indicating that accumulation of adipocytes could be closely linked with lymphatic function. Here, we propose a new antiobesity strategy based on enhancement of lymphatic and blood vessel integrity with apelin. Apelin knockout (KO) mice fed a high-fat diet (HFD) showed an obese phenotype associated with abnormal lymphatic and blood vessel enlargement. Fatty acids present in the HFD induced hyperpermeability of endothelial cells, causing adipocyte differentiation, whereas apelin promoted vascular stabilization. Moreover, treatment of apelin KO mice with a selective cyclooxygenase-2 inhibitor, celecoxib, that were fed an HFD improved vascular function and also attenuated obesity. Finally, apelin transgenic mice showed decreased subcutaneous adipose tissue attributable to inhibition of HFD-induced hyperpermeability of vessels. These results indicate that apelin inhibits HFD-induced obesity by enhancing vessel integrity. Apelin could serve as a therapeutic target for treating obesity and related diseases. *Diabetes* 62:1970–1980, 2013

O besity appears to be associated with a combination of genetic susceptibility, increased consumption of high-energy foods, and decreased physical activity, leading to excessive accumulation of white adipose tissues that serve to store surplus energy in the form of lipid within adipocytes (1). It is correlated with type 2 diabetes, cardiovascular disease, and certain types of cancer, and therefore represents a serious public health problem. Although the molecular mechanisms underlying obesity have not been fully clarified, effective therapeutic approaches are needed.

The blood and lymphatic systems are composed of dense networks of capillaries. Blood vessels are indispensable to import and carry fluid, dissolved proteins, and cells into interstitial space, whereas lymphatic vessels drain protein-rich lymph and traffic immune cells from the extracellular space (2). Adipose tissue is mainly composed of adipocytes surrounded by stromal vascular tissue. The balance of adipokine production is disrupted by excess adipose tissue, leading to chronic vascular inflammation, which in turn may lead to cardiovascular disease (3). The outgrowth of adipose tissue is tightly correlated with angiogenesis (4). Thus, antiangiogenesis therapy has emerged as a potential treatment of obesity. However, this idea remains controversial not only because angiogenesis is physiologically important but also because brown adipose tissue consumes more energy if angiogenesis is increased (5). Moreover, there is an increasing emphasis on lymphatic function in obesity research. *Chy* mice, a naturally occurring mouse model of lymphedema attributable to heterozygous inactivating mutations in vascular endothelial growth factor receptor (VEGFR)-3, exhibit adipose layer accumulation (6). Also, surviving Prox1 heterozygous mice show abnormal lymphatic patterning and adult-onset obesity (7). Thus, accumulation of adipocytes could be closely linked with the structure and function of lymphatic vessels. However, little is known about how vessel integrity influences adipocyte dynamics.

The apelin gene encodes a 77-amino-acid preprotein, which is cleaved to shorter active peptides that bind to the apelin receptor (APJ), a G-protein-coupled receptor (8). The full-length mature peptide comprises 36 amino acids (apelin-36), and other active fragments, including a 13-amino-acid peptide known as apelin-13, also are formed. Apelin is expressed widely in the vascular endothelium and acts both locally and via endocrine signaling to activate APJ, which is expressed in cardiomyocytes, endothelial cells, and vascular smooth muscle cells (9). Apelin/APJ signaling is located downstream of angiopoietin-1/Tie2 signaling in endothelial cells (10). Apelin transgenic mice develop enlarged, but not leaky, blood vessels in ischemia, leading to functional recovery (11). More recently, we have shown that apelin attenuates edema formation and inflammation by promoting lymphatic function in vivo (12).

Herein, we show that the apelin/APJ system enhances the integrity of lymphatic and blood vessels exposed to dietary fatty acids, resulting in inhibition of high-fat diet (HFD)-induced obesity. These results suggest that apelin may be a new therapeutic target in the treatment of obesity and its related diseases.

RESEARCH DESIGN AND METHODS

Animals. Male and female apelin-deficient mice (knockout [KO]) and apelin transgenic mice under the control of keratin 14 on a C57/BL6 background (K14-apelin) were generated as described previously (11). All animals were housed in groups (n = 3–10) in a temperature-controlled room with a 12-h/12-h light–dark cycle. Both wild-type (WT) and KO mice (7–11 weeks old) were maintained on HFD (D12492, 60 kcal % fat; Research Diets, New Brunswick, NJ) for 17 weeks. In other studies, WT and KO mice fed the same HFD were further divided into two groups (n = 3–7) cotreated with vehicle or 0.1% selective cyclooxygenase (COX) 2 inhibitor celecoxib (CEL; LC Laboratories, Woburn, MA) from the age of 7–8 weeks for 8 weeks. Moreover, K14-apelin and WT mice at age 4–5 weeks were fed HFD (D12451, 45 kcal % fat; Research Diets)

for 8 weeks. Mice had free access to food and water. We measured body weight and the mass of food consumed every week. At the end of the study, we weighed the inguinal and mesenteric fat pads and collected the ears, back skin, and mesenteric fat for histological analysis, and collected blood samples for analysis of the circulating levels of glucose, triglyceride, free fatty acids, HDL cholesterol, insulin, leptin, and adiponectin. Plasma of HR-1 hairless mice fed a regular diet (RD; CRF-1; Oriental Yeast, Tokyo, Japan) or HFD (D12492, 60 kcal % fat; Research Diets) for 11 weeks also was collected. The current study was approved by the Ethics Committee of Shiseido Research Center in accordance with the guidelines of the National Institute of Health.

Immunohistochemical and computer-assisted morphometric vessel analysis. Immunofluorescence analysis was performed on 6-μm cryostat sections of mouse back skin or 12-μm cryostat sections of mesenteric fat using antibodies against the macrophage monocyte marker CD11b (BD Biosciences, Bedford, MA), the blood vessel–specific marker meca-32 (BD Biosciences), the lymphatic-specific marker LYVE-1 (MBL, Nagoya, Japan), podoplanin (AngioBio, Del Mar, CA), APJ (10), perilipin (PROGEN Biotechnik GmbH, Heidelberg, Germany), Ki-67 antigen (Dako Cytomation, Glostrup, Denmark), and corresponding secondary antibodies labeled with AlexaFluor488 or AlexaFluor594 (Molecular Probes, Eugene, OR). Routine hematoxylin and eosin staining also was performed. Sections were examined with an Olympus AX80T microscope (Olympus, Tokyo, Japan) and images were captured with a DP-controlled digital camera (Olympus). Morphometric analyses were performed using the IP-LABORATORY software as described (13). Three different fields of each section were examined and the number of macrophages and the average vessel size in the dermis and in the mesenteric fat were determined. Whole-mount immunohistochemical analysis of ear skin was performed. Tissues were incubated in 30% H_2O_2, 3% normal goat serum (Invitrogen, Camarillo, CA), and 0.25% Triton X-100 in PBS, and incubated overnight at 4°C with anticlaudin-5 antibody (Santa Cruz Biotechnology, Santa Cruz, CA) or anti-CD31 antibody (BD Biosciences), as an endothelial marker, and anti-podoplanin antibody (AngioBio, Del Mar, CA) or anti-LYVE-1 antibody, as a lymphatic marker. Then, corresponding secondary antibodies labeled with AlexaFluor488 or AlexaFluor594 (Molecular Probes) were applied. Specimens were viewed with a LSM5 Pascal confocal laser-scanning microscope (Carl Zeiss, Thornwood, NY).

Adipose tissue imaging. Adipose tissue imaging of inguinal fat was performed as described previously (14). The inguinal subcutaneous fat was minced into small pieces and incubated with BODIPY (4,4-difluoro-3a,4a-diaza-s-indacene) conjugated with Alexa Fluor (Invitrogen-Molecular Probes, Carlsbad, CA) as a lipid droplet marker and Isolectin IB$_4$ Alexa Fluor dye conjugates (Invitrogen-Molecular Probes) as an endothelial marker. The three-dimensional structure of adipocytes was observed using a LSM5 Pascal confocal laser-scanning microscope (Carl Zeiss). Adipocyte diameter was determined using IPLab software. Four image fields were acquired from three animals in each group, and the diameters of 20 cells in each field were measured by an observer blinded regarding the status of the sample. Adipocytes were defined as regular, round, BODIPY$^+$ cells without plasma membrane disruption.

Blood analysis. Plasma glucose, HDL cholesterol, and triglyceride levels were measured using a Fuji DRI-CHEM analyzer (Fuji Film, Tokyo, Japan). Plasma free fatty acid level was determined with a Wako NEFA C test kit (Wako Chemicals, Neuss, Germany). Insulin, leptin, and adiponectin were assayed with a mouse insulin ELISA kit (Shibayagi, Gunma, Japan) and a leptin and adiponectin ELISA kit (R&D Systems, Minneapolis, MN), respectively, according to the manufacturers' instructions.

Plasma extravasation and lymphatic functional analysis. To examine the blood vascular permeability, Miles assay was performed as previously described (11). Briefly, mice were anesthetized and intravenously injected with 100 μL of a 1% solution of Evans blue dye in 0.9% NaCl. At 30 min after dye injection, pictures were taken and the epididymal fat was removed. The dye was eluted from dissected samples with formaldehyde at 56°C and the optical density was measured by spectrophotometry (Biotrak II; GE Healthcare, Fairfield, CT) at 620 nm. For lymphatic functional analysis, a 1-μl aliquot of 1% solution of Evans blue dye in 0.9% NaCl was injected intradermally at the inner surface of the rim of the ear using a 10-μL Hamilton syringe; this is a standard method to macroscopically visualize cutaneous lymphatic vessels and lymphatic drainage. Mouse ears were photographed at 1 and 5 min after the dye injection. Additionally, 100 μL of 1% solution of Evans blue dye in 0.9% NaCl was injected into the stomach and at 30 min after dye injection, the mesenteric fat was carefully removed from the intestine. The optical density of the eluted dye in the mesenteric fat was measured.

Cells. Human dermal lymphatic endothelial cells (LECs) were isolated from neonatal human foreskins by immunomagnetic purification as described previously (15). Lineage-specific differentiation was confirmed by real-time RT-PCR for the lymphatic vascular markers Prox1, LYVE-1, and podoplanin, as well as by immunostaining for Prox1 and podoplanin as described (13). Human umbilical vein endothelial cells were purchased (PromoCell, Heidelberg,

Germany) and cultured in endothelial basal medium (Lonza, Verviers, Switzerland) with supplements provided by the suppliers for up to 11 passages. Primary human subcutaneous preadipocytes (Lonza) were cultured as recommended by the supplier in preadipocyte basal medium 2 containing 10% FBS, 2 mmol/L L-glutamine, and antibiotics. The 3T3-L1 preadipocytes were cultured in DMEM with 10% FBS and antibiotics.

Permeability assay. LECs and human umbilical vein endothelial cells were grown to confluence on the fibronectin-coated surface of 0.4-μm pore-size tissue culture inserts (Corning, Lowell, MA). Oleate (20 or 100 μmol/L) and stearate (20 or 100 μmol/L) were placed into the upper and lower chambers for 5 h after incubation with apelin-13 (1,000 ng/mL) or a selective COX2 inhibitor, CEL (1 μmol/L), for 1 h. FITC-dextran was added to the upper chambers, and the apparatus was then placed in a CO_2 incubator at 37°C. After incubation for 15 min, a 100-μL sample was taken from the lower chamber and the absorbance of FITC-dextran was determined at 492 nm using a spectrophotometer (Fluoroskan Ascent; Thermo Fisher Scientific, Waltham, MA).

Adipocyte differentiation assay. Differentiation of 3T3-L1 preadipocytes was performed by treatment with insulin, dexamethasone, and 3-isobutyl-1-methylxanthine in DMEM with 10% FBS for 2 days as described (16). Then, the medium was replaced with DMEM containing 10% FBS and insulin before coculture with LECs. Coculture was performed by incubating LECs to confluence on the 0.4-μm pore-size cell culture insert (Corning) and placing them in 6-well plates containing 3T3-L1 adipocytes differentiated for 2 days; 0.5% plasma from mice fed RD or HFD for 11 weeks was added to the upper chambers. After incubation for 7 days, the cells in the lower wells were stained with Oil-Red-O (Wako Pure Chemical Industry, Osaka, Japan) as described previously (17). The stained lipids present in the mature adipocytes were solubilized with isopropanol and measured spectrophotometrically at 510 nm. To induce differentiation of human preadipocytes into mature adipocytes, confluent preadipocytes in plates were cultured in preadipocyte basal medium 2 plus 10% FBS, 2 mmol/L glutamine, and antibiotics for 2 days and then switched to preadipocyte basal medium 2 plus 10% FBS, 2 mmol/L glutamine, antibiotics, 10 μg/mL insulin, 500 μmol/L isobutylmethylxanthine, 1 μmol/L dexamethasone, and 200 μmol/L indomethacin in the presence or absence of oleate (100 μmol/L) and stearate (100 μmol/L). After 9 days of incubation, cells were fixed with 10% formaldehyde, stained with Oil-Red-O (Wako Pure Chemical Industry) and observed under a bright-field microscope (Olympus) as described previously (17).

Immunofluorescence microscopy. LECs and human umbilical vein endothelial cells were seeded on cover slips and incubated until confluence. For the detection of VE-cadherin, cells were fixed with 1% PFA and incubated with anti-VE-cadherin antibody (R&D Systems, Minneapolis, MN). AlexaFluor594-labeled secondary antibody was used for fluorescence detection. All images were acquired using a DP-controlled digital camera (Olympus) on an Olympus AX80T microscope (Olympus).

Quantitative real-time RT-PCR. Total RNAs were isolated from LECs cultured in the presence or absence of apelin (1,000 ng/mL) for 4 h after serum starvation. The expression of COX2 mRNA was examined by quantitative real-time RT-PCR using a LightCycler 480 (Roche Applied Science, Indianapolis, IN). The primers for COX2 were as follows: forward primer, 5′- TAGAGC-CCTTCCTCCTGTGC-3′, and reverse primer, 5′- CTGGGCAAAGAATGCAAA-CA-3′. Expression levels were normalized with respect to β-actin as an internal control (forward primer: 5′-TCACCGAGCGCGGCT-3′; reverse primer: 5′-TAATGTCACGCACGATTTCCC-3′).

Statistical analysis. All data are expressed as means ± SD and as the statistical significance of differences with an unpaired t test.

RESULTS

Disruption of apelin/APJ signaling in vivo promotes obesity. To investigate the physiological role of apelin in obesity, apelin KO mice were fed HFD. Surprisingly, after 5 weeks of HFD, apelin KO mice showed increased body weight compared with WT littermates (Fig. 1A); at the end of the feeding period, the body weight gains were 20 ± 0.5 g for WT mice and 30 ± 0.5 g for apelin KO mice ($P <$ 0.01) (Fig. 1B). As expected, both inguinal subcutaneous and mesenteric fat depots were significantly increased by HFD in apelin KO mice compared with WT mice (Fig. 1C, D). Moreover, hematoxylin and eosin staining revealed a thickened subcutaneous adipose layer in the skin of HFD-fed apelin KO mice as compared with WT mice (Fig. 1E). To visualize the three-dimensional structure of adipose tissue, we used fluorescence staining with BODIPY, which recognizes intercellular lipid droplets in
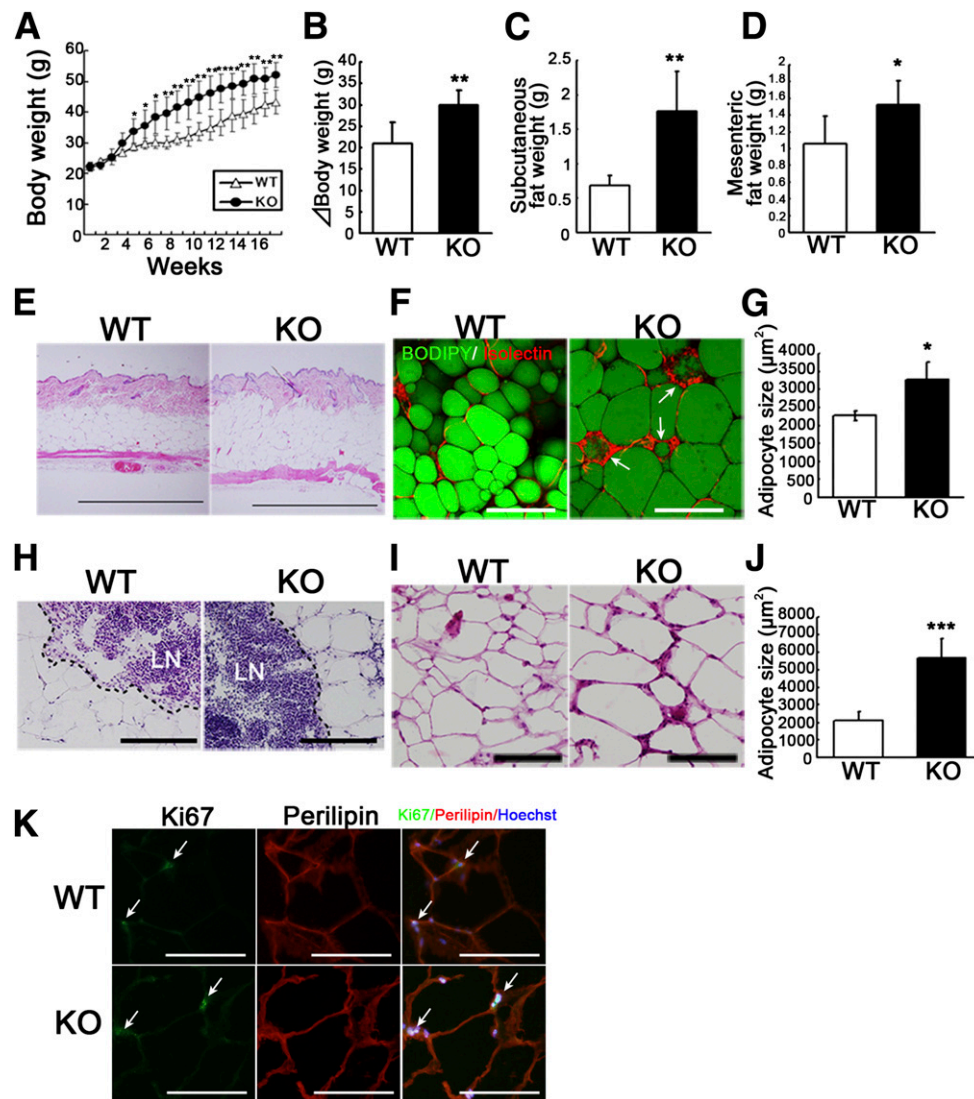
FIG. 1. Obesity in HFD-fed apelin KO mice. *A*: Body weight of HFD-fed apelin KO and WT mice (*N* = 7). Increased body weight (*B*), inguinal subcutaneous fat weight (*C*), and mesenteric fat weight (*D*) in apelin KO mice after 17 weeks of HFD. *E*: Hematoxylin and eosin staining showed a thickened subcutaneous fat layer in apelin KO mice. BODIPY (green) and Isolectin (red) staining revealed increased lipid droplet (green) size in subcutaneous adipocytes in apelin KO mice (*F*). Morphometric analysis of adipocyte size confirmed enlargement of adipocytes in apelin KO mice (*G*). Arrows show crown-like structures in obese fat pads. Hematoxylin and eosin staining of subcutaneous adipose tissue surrounding lymph nodes (LN) (*H*) and of mesenteric fat tissue (*I*). *J*: Morphometric analysis of mesenteric adipocyte size. Bars indicate 200 μm except in (*E*), which shows 1 mm. Date are expressed as mean values ± SD. *K*: Double immunofluorescence staining with Ki67 (green) and perilipin (red) in the mesenteric fat of WT and apelin KO mice after HFD. Arrows show proliferating adipocytes. ****P* < 0.001, ***P* < 0.01, **P* < 0.05.

adipocytes. Subcutaneous adipocytes in HFD-fed apelin KO mice were increased in size (Fig. 1*F*) and surrounded by endothelial cells, which appeared to form crown-like structures in obese fat pads, as described previously (14). Morphometric analysis confirmed that adipocytes were enlarged in the HFD-fed apelin KO mice (Fig. 1*G*). Sections of subcutaneous white adipose tissue around lymph nodes and sections of mesenteric fat tissue showed increased adipocyte size of apelin KO mice as compared with controls (Fig. 1*H–J*). Double immunofluorescence staining using antibodies against proliferation marker Ki67 and perilipin revealed no significant difference of proliferating adipocytes in mesenteric fat tissues between apelin KO mice and WT mice after HFD (Fig. 1*K*).

No major abnormality of food consumption or lipid metabolism in apelin KO mice. Because apelin/APJ signaling in the central nervous system contributes to body

fluid homeostasis (18), we investigated the food consumption of HFD-fed apelin KO mice to determine if the obese phenotype of apelin KO mice was elicited by abnormality of hypothalamic function after HFD feeding. There was no significant difference in the amount of weekly food intake between apelin KO mice and their WT littermates (Fig. 2*A*). The plasma insulin level in obese apelin KO mice was slightly, but not significantly, decreased as compared with WT mice (Fig. 2*B*). However, the leptin concentration in apelin KO mice was significantly increased, whereas the adiponectin level was significantly decreased (Fig. 2*C, D*). We also measured the levels of circulating glucose, HDL cholesterol, triglycerides, and free fatty acids in the plasma of obese apelin KO mice and their WT counterparts but found no significant difference in any of these factors (Fig. 2*E–H*).

Abnormal lymphatic dysfunction and inflammation in skin of HFD-fed apelin KO mice. To examine infiltration of macrophages in the adipose tissue, we used immunohistochemical staining for CD11b. The results demonstrated an increase of infiltrating macrophages in the subcutaneous adipose layer of HFD-fed apelin KO mice, as compared with WT mice (Fig. 3A). Morphometric analysis confirmed an increased number of infiltrating macrophages in the subcutaneous adipose tissue of apelin KO mice ($P < 0.01$) (Fig. 3B). We have previously demonstrated that apelin promotes lymphatic function during inflammation (12). Therefore, to determine whether apelin depletion could lead to vascular abnormality in obese

mice, we examined the expression of the APJ in lymphatic and blood vessels in vivo. Double immunofluorescence staining for the lymphatic marker podoplanin or the vascular marker meca-32 and APJ revealed weak APJ expression in cutaneous lymphatic vessels from mice fed RD, whereas HFD-fed mice showed increased expression of APJ in LECs (Fig. 3C). In contrast, APJ expression levels were similar in blood vessels of RD-fed and HFD-fed mice (Fig. 3D). Given these data, we speculated that disruption of apelin signaling resulted in abnormal structure of lymphatic or blood vessels and increased their leakiness. Lymphatic and blood vessels in dermis of HFD-fed apelin KO mice were clearly enlarged (Fig. 3E), and the diameter of lymphatic and blood vessels was increased compared with those in WT controls (Fig. 3F). In addition, to analyze the enlarged lymphatic structure in apelin KO mice, whole-mount immunofluorescence for claudin-5 also was performed. We confirmed that the large vessels stained for claudin-5 were lymphatic marker podoplanin-positive vessels (Fig. 3G). Whole-mount immunofluorescence for claudin-5 of ear skin from HFD-fed WT and apelin KO mice also revealed dilation of lymphatic vessels in apelin KO mice (Fig. 3G). Surprisingly, obese apelin-KO mice showed not only angiogenesis but also lymphatic hyperplasia in the subcutaneous fat layer, whereas this was not the case in subcutaneous adipose tissue of HFD-fed WT mice (Fig. 3H). Functional analyses by means of intradermal injection of Evans blue dye into mouse ears revealed lymphatic backflush and leakiness in HFD-fed apelin KO mice as compared with WT mice (Fig. 3I).

Dietary fatty acids cause hyperpermeability of lymphatic and blood vessels and adipocyte hypertrophy. To understand the mechanism through which HFD-fed apelin KO mice developed significant obesity, we investigated in vitro the effects of dietary fatty acids on LECs. The 3T3-L1 preadipocytes were cocultured with confluent LECs on Transwell inserts in the presence of plasma from HFD-fed or RD-fed WT mice to mimic the lymphatic endothelial wall (Fig. 4A). Surprisingly, the amount of lipid droplets was increased in the presence of plasma from HFD-fed mice, whereas no major difference was found in the presence or absence of plasma from RD-fed mice (Fig. 4B, C). Because significant increases of oleic acid and stearic acid were found in plasma of HFD-fed mice (M. Takagi, unpublished observation), we speculated that the elevated fatty acids in plasma of HFD-fed mice would induce dysfunction of lymphatic and blood vessels via apelin depletion, thereby promoting obesity. Treatment of LECs with 20 and 100 μmol/L oleic acid resulted in hyperpermeability of LECs compared with untreated cells (Fig. 4D). Moreover, we confirmed that these dietary fatty acids promoted differentiation of human subcutaneous adipocytes (Fig. 4E). Preincubation with apelin-13 blocked the hyperpermeability of lymphatic and blood vessel endothelial cells induced by oleic acid (Fig. 4F, G). Moreover, whereas unstimulated endothelial cells were stained evenly with VE-cadherin at sites of cell–cell junctions, cells incubated with oleic acid displayed discontinuous staining with considerable gaps. Surprisingly, cells pretreated with apelin-13 before incubation with oleic acid retained the normal staining pattern of VE-cadherin (Fig. 4H). These data indicate that the oleic acid in HFD enhances the leakiness of lymphatic and vascular structures via disruption of VE-cadherin, and that leakage of dietary fatty acids from the vessels mediates adipocyte hypertrophy.
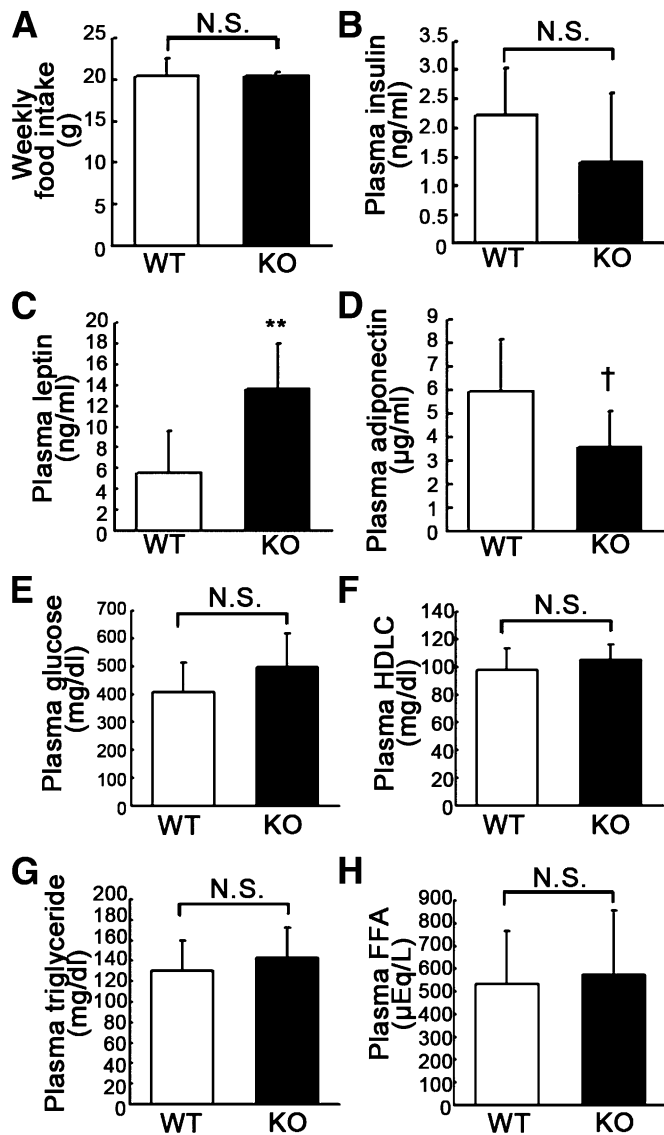
FIG. 2. No significant difference was found in food consumption or lipid metabolism between apelin KO and WT mice after HFD. *A:* Food intake was similar in apelin KO mice and WT littermates. *B:* Obese apelin KO mice had a lower plasma insulin level, but the difference was not significant. *C:* Serum leptin levels were approximately two times higher in apelin KO mice than in WT mice (**$P < 0.01$). *D:* Serum adiponectin levels tended to be lower in apelin KO mice, but the difference was not significant. There was no significant difference of plasma glucose (*E*), HDL cholesterol (HDLC; *F*), triglyceride (*G*), or free fatty acid (FFA; *H*) between apelin KO mice and WT mice. Data are expressed as mean values ± SD ($N = 7$; **$P < 0.01$, †$P < 0.1$). N.S., not significant.
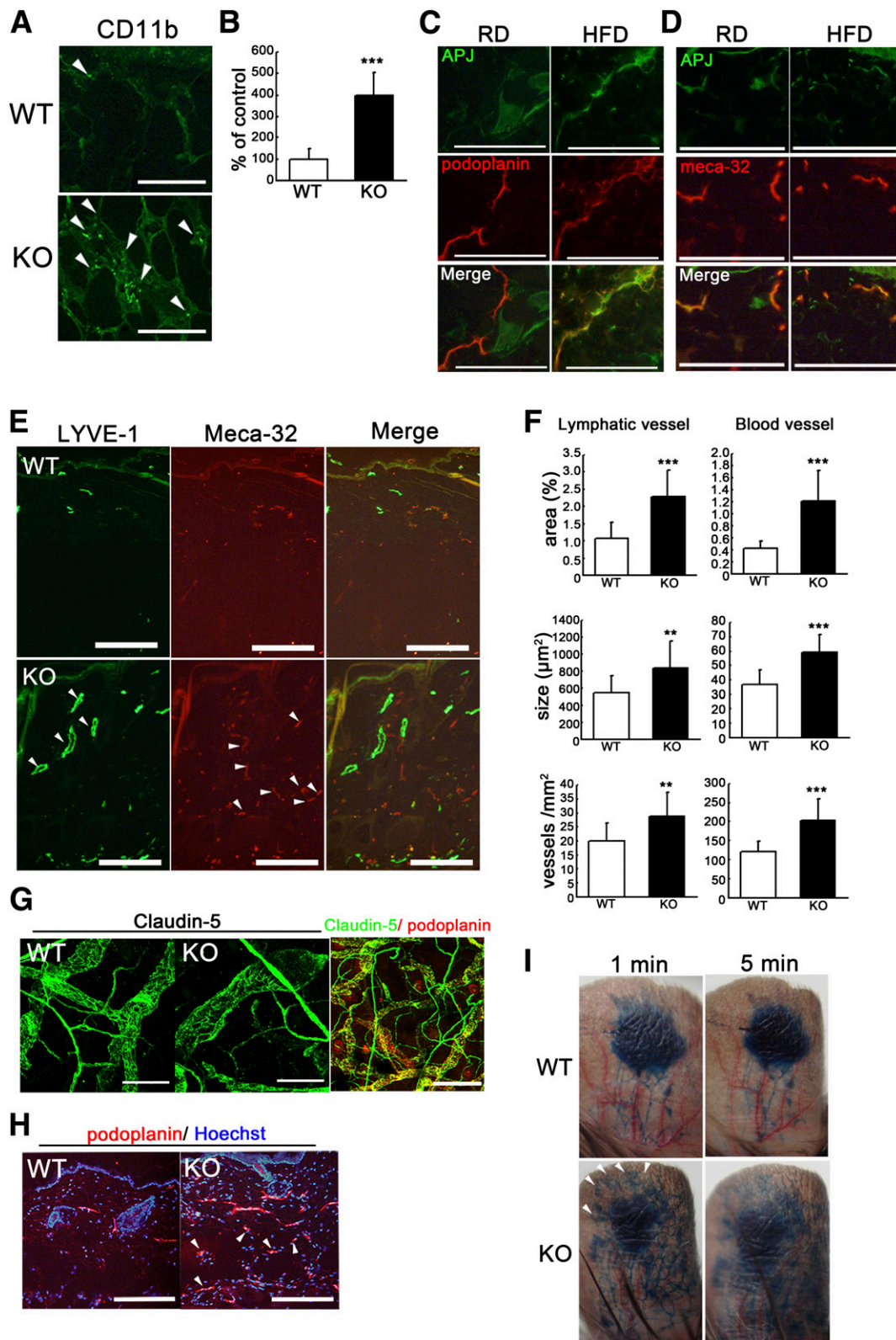
FIG. 3. Enhanced inflammation and vascular malformation in obese apelin KO mice. *A*: Increased CD11b^{+} macrophages (green) in the subcutaneous adipose layer of skin from apelin KO mice. *B*: Morphometric analysis showed that the number of CD11b^{+} macrophages was significantly increased in apelin KO mice. Double immunofluorescence staining for podoplanin (*C*, red) or meca-32 (*D*, red) and for APJ (green) revealed upregulated expression of APJ in lymphatics of skin of HFD-fed mice. *E*: Double immunofluorescence staining of skin for LYVE-1 (green) and meca-32 (red) revealed enlargement (arrowheads) and enhanced formation of LYVE-1^{+} lymphatic vessels and meca-32[+] blood vessels in apelin KO mice. *F*: Computer-assisted morphometric analyses of lymphatic and blood vessels in skin. *G*: Immunofluorescence staining for claudin-5 in a whole-mount of ear skin. Lymphatic vessels in apelin KO mice were partly dilated compared with controls. Double immunofluorescence staining of claudin-5 (green) and podoplanin (red) confirmed that the nonuniform vessels were podoplanin-positive lymphatic vessels. *H*: Immunofluorescence analysis of mouse skin for podoplanin (red) revealed lymphatic hyperplasia in the adipose layer of apelin KO mice. *I*: Intradermal injection of Evans blue dye visualized enhanced leakiness of enlarged lymphatic vessels and lymphatic backflush (arrowheads) in apelin KO mice at 1 and 5 min after the injection. Scale bars indicate 200 μm except in (*G*), which indicates 100 μm. Data are expressed as mean values ± SD. **$P < 0.01$, ***$P < 0.001$.
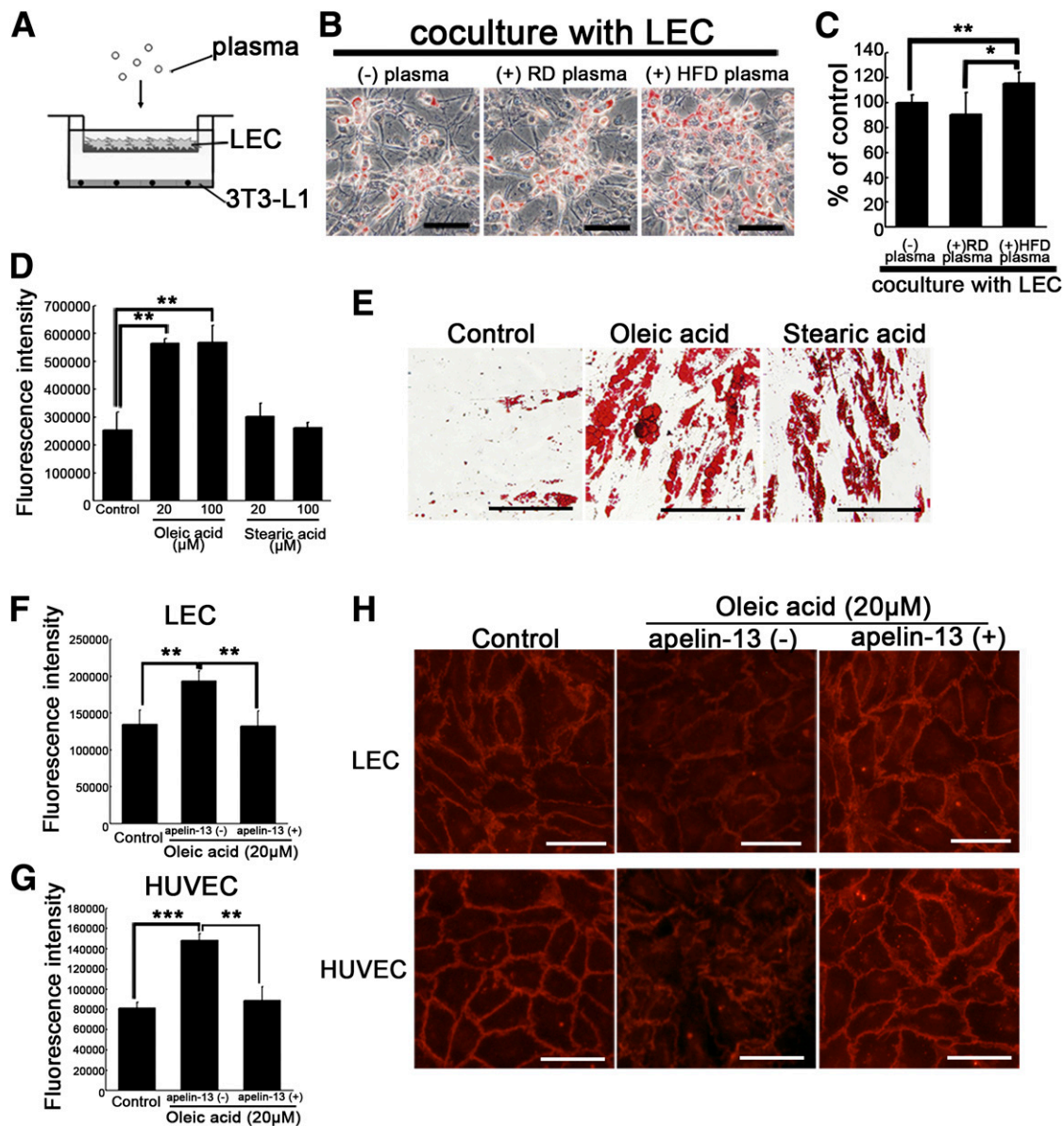
FIG. 4. Apelin inhibits vascular hyperpermeability induced by oleic acid, thereby blocking adipocyte differentiation. *A*: Schematic illustration of coculture study of LECs with 3T3-L1 preadipocytes in the presence or absence of plasma. Confluent LECs were inserted with or without plasma on day 2 after initiation of differentiation. *B*: 3T3-L1 preadipocytes were stained with Oil-red-O (red) on day 9 after initiation of differentiation. *C*: Quantitative evaluation of lipid droplets of 3T3-L1 preadipocytes. *D*: Treatment with oleic acid increased the fluorescence intensity of permeated FITC-dextran from LECs, as compared with the control. *E*: Human subcutaneous preadipocytes were stained with Oil-red-O (red) on day 9 after initiation of differentiation with oleic acid or stearic acid. Fatty acid–exposed culture showed an increased amount of lipid droplets compared with the control. The addition of apelin-13 blocked the hyperpermeability of LECs (*F*) and human umbilical vein endothelial cells (HUVECs; *G*) induced by oleic acid. *H*: Immunohistochemistry of VE-cadherin (red) in LECs and HUVEC, showing discontinuous staining of VE-cadherin after incubation with oleic acid. Apelin-13 blocked the discontinuity of staining of VE-cadherin and the gap formation induced by oleic acid. Scale bars indicate 200 μm (*E*) and 100 μm (*B* and *H*). Data are expressed as mean values ± SD. *$P < 0.05$, **$P < 0.01$, ***$P < 0.001$.

A selective COX2 inhibitor blocked the disruption of apelin/APJ signaling. To determine how the lymphatic and vascular systems affect HFD-induced obesity in vivo, we treated HFD-fed apelin KO mice with a selective COX2 inhibitor, CEL. It has been shown that COX2 inhibitors block angiogenesis and lymphangiogenesis during tumor growth (19). The CEL-treated, HFD-fed, apelin KO mice gained 30% less weight than HFD-fed apelin KO mice, and showed differences in subcutaneous and mesenteric fat accumulation (Fig. 5*A–D*). Hematoxylin and eosin staining of skin sections confirmed a decreased adipose layer in the CEL-treated apelin KO mice, with a decreased adipocyte diameter (Fig. 5*E, F*). However, no significant difference in

weight gain or fat accumulation was found between WT mice fed with and without CEL (Fig. 5*A–D*). Immunohistochemical analyses revealed that CEL blocked enlargement of lymphatic and blood vessels in HFD-fed apelin KO mice (Fig. 5*G*), and morphometric analysis confirmed that the vessel size was decreased (Fig. 5*H*). Moreover, fat pads from CEL-treated, HFD-fed, apelin KO mice showed decreased CD11b$^+$ macrophages (Fig. 5*I*). CEL-treated, HFD-fed, apelin KO mice showed a decreased number of macrophages in subcutaneous adipose tissue (Fig. 5*J*). Further, CEL blocked the lymphatic and blood vascular hyperpermeability induced by oleic acid, like apelin-13 (Fig. 5*K*). In contrast, COX2 expression in LECs was
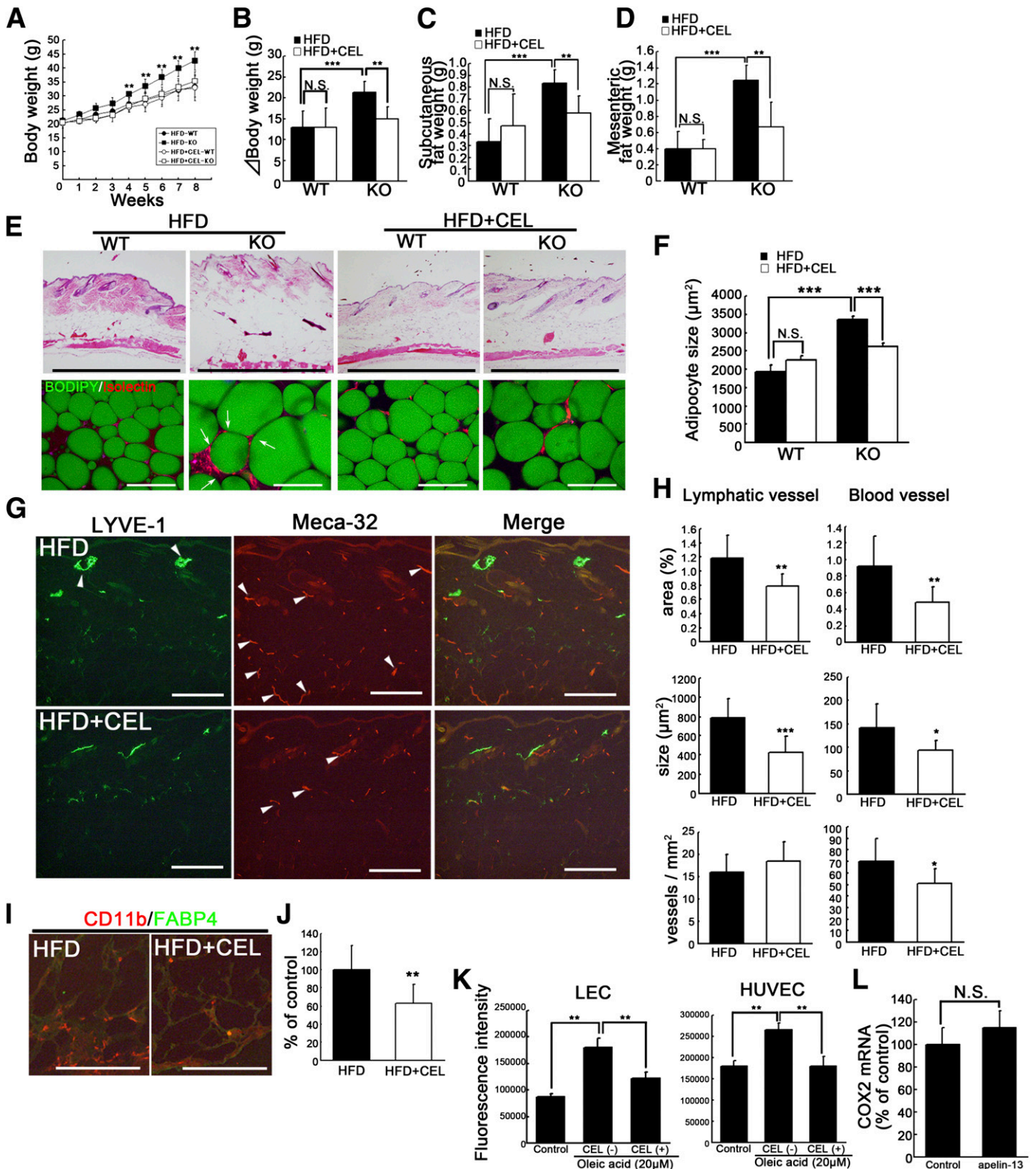
FIG. 5. Obesity induced by apelin depletion after HFD was blocked by orally administered selective COX2 inhibitor. A: Weight gain in WT and apelin KO mice maintained on HFD or HFD containing CEL ($N = 3–7$). The change of body weight (B) and tissue weight of inguinal subcutaneous (C) and mesenteric (D) fat after HFD or HFD with CEL. E: Histological analysis of skin and subcutaneous adipose tissue imaging using BODIPY (green) and Isolectin (red) showed that hypertrophic adipocytes (green) were reduced in CEL-treated HFD-fed apelin KO and WT mice. Arrows show crown-like structures in obese fat pads. F: Mean adipocyte size in CEL-treated, HFD-fed, apelin KO mice was smaller than in HFD-fed apelin KO mice. G: Immunohistochemical analyses for LYVE-1 (green) and meca-32 (red) revealed that enlargement of lymphatic and blood vessels (arrowheads) in the skin of HFD-fed apelin KO mice was inhibited by CEL. H: Morphometric analyses of lymphatic and blood vessels in CEL-treated, HFD-fed, apelin KO mice and HFD-fed apelin KO mice. I: Double immunofluorescence staining for CD11b (red) and FABP4 (green) showed that macrophage infiltration in the subcutaneous fat layer from HFD-fed apelin KO mice was blocked by CEL. J: The number of infiltrated macrophages was decreased in apelin KO mice fed HFD with CEL. K: Increased permeability in LECs and human umbilical vein endothelial cells (HUVECs) after the treatment with oleic acid was blocked by the addition of CEL. Bars indicate 1 mm (E, top) and 200 μm (E, bottom, G, and I). Data are expressed as mean values ± SD. L: COX2 expression after apelin treatment of LECs. ***$P < 0.001$, **$P < 0.01$, and *$P < 0.05$.

similar in controls and apelin-treated cells (Fig. 5*L*). Taken together, these results show that the selective COX2 inhibitor CEL ameliorated both inflammation and the dysfunction of lymphatic and blood vessels in HFD-fed apelin KO mice, resulting in the inhibition of HFD-induced obesity.

Resistance to obesity in apelin transgenic mice. To examine whether the stabilization of lymphatic and blood vessels by apelin inhibits the accumulation of fat tissue, we used apelin transgenic mice under the control of K14 (K14-apelin). Interestingly, HFD-fed K14-apelin mice showed significant inhibition of weight gain and decreased accumulation of subcutaneous adipose tissue as compared with HFD-fed WT mice, although there was no significant difference of weekly food intake between the two groups (Fig. 6*A*, *B*). The adipose layer of skin and the amount of subcutaneous adipose tissue in HFD-fed K14-apelin mice were decreased (Fig. 6*C*, *D*). Morphometric analysis also confirmed a decrease of lipid droplets within adipocytes in K14-apelin mice (Fig. 6*E*). Next, lymphatic function in the mesenteric fat was analyzed by injecting dye into the stomach, revealing the inhibition of lymphatic hyperpermeability in K14-apelin mice as compared with WT mice (Fig. 6*F*). To evaluate the structural change of lymphatic and blood vessels, we performed whole-mount staining for LYVE-1 (green)/meca-32 (red) in ears of mice. Interestingly, both blood and lymphatic vessels of WT mice were enlarged after HFD, whereas the diameters of blood and lymphatic vessels were comparable between RD- and HFD-fed K14-apelin mice (Fig. 6*G*). These results are consistent with the idea that apelin regulates the accumulation of adipose tissue by promoting vessel integrity.

Structural and functional change of vessels in the adipose tissues of K14-apelin and KO mice after HFD. Miles assay was performed to determine of the effect of apelin on blood vessels in epididymal fat. We found that leakiness was inhibited in K14-apelin mice and enhanced in apelin KO mice after HFD (Fig. 7*A*). Quantitative analysis showed that HFD enhanced dye leakage in WT mice, whereas the increase of dye leakage was inhibited in K14-apelin mice. In contrast, dye leakage was strongly enhanced in apelin KO mice after HFD (Fig. 7*B*).

Immnofluorescence analysis was performed with antibodies for blood vessels (Fig. 7*C*) and lymphatic vessels (Fig. 7*E*). HFD induced enlargement of lymphatic and blood vessels of WT mice as compared with RD-fed WT mice. Moreover, lymphatic vessels as well as blood vessels were markedly enlarged in HFD-fed apelin KO mice. Morphometric analysis of lymphatic and blood vessels confirmed an increase in the average size of lymphatic vessels of HFD-fed WT mice as compared with RD-fed WT mice. Importantly, HFD induced marked enlargement of both blood and lymphatic vessels in apelin KO mice. In contrast, no significant difference of blood vessels was found between RD- and HFD-fed WT mice (Fig. 7*D*, *F*).

DISCUSSION

Our results indicate that apelin/APJ signaling plays a crucial role in the control of fat accumulation by enhancing the integrity of lymphatic and blood vessels. It is well-established that fat intake is associated with the growth of adipose tissue vasculature. This, in turn, suggests that inhibition of angiogenesis in adipose tissue could be an approach to treat obesity, but this idea is controversial because of the physiological importance of angiogenesis. It was reported that partial blockade of the VEGFR pathway

had no effect on diet-induced obesity (5). Additionally, recent reports indicated that blocking the VEGFR-3 pathway in skin resulted in an increase of subcutaneous adipose tissue (20), and that Prox1 heterozygous mice showed obesity and abnormal lymphatic function, particularly at the mesentery and thoracic duct (7). These results suggest that there is a link between lymphatic function and adipose tissue accumulation. Here, we propose that a strategy of enhancing the integrity of lymphatic and blood vessels could be a novel approach to antiobesity therapy.

Although HFD-fed apelin KO mice showed a markedly obese phenotype accompanied by dysfunction of lymphatic and blood vessels, it was also found that there was no significant difference of either vessel function or fat accumulation between apelin KO and WT mice fed a normal diet. These results led us to hypothesize that dietary fatty acids accelerate vascular damage via apelin depletion, because fatty acids are absorbed by lymphatic vessels and transported to peripheral tissues by blood vessels. Our in vitro study demonstrated that plasma from HFD-fed mice increased the amount of lipid droplets of 3T3-L1 preadipocytes by disrupting lymphatic integrity and that oleic acid, a dietary fatty acid, directly mediates hyperpermeability of endothelial cells by disrupting adherens junctions. Apelin is required for the assembly of functional vasculature during angiogenesis (11). Interestingly, apelin inhibited oleic acid–induced vascular hyperpermeability by modulating VE-cadherin in vitro. Taken together, these results indicate that HFD-fed apelin KO mice develop abnormal vascular leakiness and structure as a result of the synergistic effects of apelin depletion and increase of oleic acid. Importantly, lymphatic backflush and abnormal leakiness were found in the ear skin of HFD-fed apelin KO mice. In vitro, lymphatic permeability was induced in the presence of fatty acids, whereas apelin attenuated the fatty acid–induced hyperpermeability. Because leakiness and structural abnormalities of skin lymphatic vessels are seen in apolipoprotein E–deficient mice (21), these results suggest that abnormal transportation and lymphatic absorbance of fatty acids from peripheral tissues like skin could be involved in the development of obesity. Moreover, lymphatic hyperplasia was found in the subcutaneous fat layer from extremely obese apelin KO mice in contrast to normal and obese WT mice. In inflamed skin, increased interstitial fluid pressure caused by increased leakage from blood vessels may increase fluid drainage through lymphatic vessels, but this may impair lymphatic function (22). Thus, an increase of lymphatic vessels could facilitate lymphatic drainage and resolution of the related inflammation (23,24). Therefore lymphangiogenesis in adipose tissue could be a significant therapeutic target, although further study is needed to determine whether infiltrated macrophages in obese adipose tissue or mature adipocyte-derived VEGF-C are involved in the promotion of lymphangiogenesis in adipose tissue.

What is the role of apelin in obesity? In vivo, an orally administered COX2 inhibitor rescued apelin KO mice from HFD-induced obesity. A COX2 inhibitor directly affects vascular function, suppressing angiogenesis and lymphangiogenesis associated with tumor growth (19). The COX2 inhibitor, CEL, blocked angiogenesis and blood/lymphatic vessel enlargement in HFD-fed apelin KO mice. In vitro, we found that CEL treatment blocked oleic acid–induced hyperpermeability of lymphatic and blood vessel endothelial cells. Taken together with the fact that several
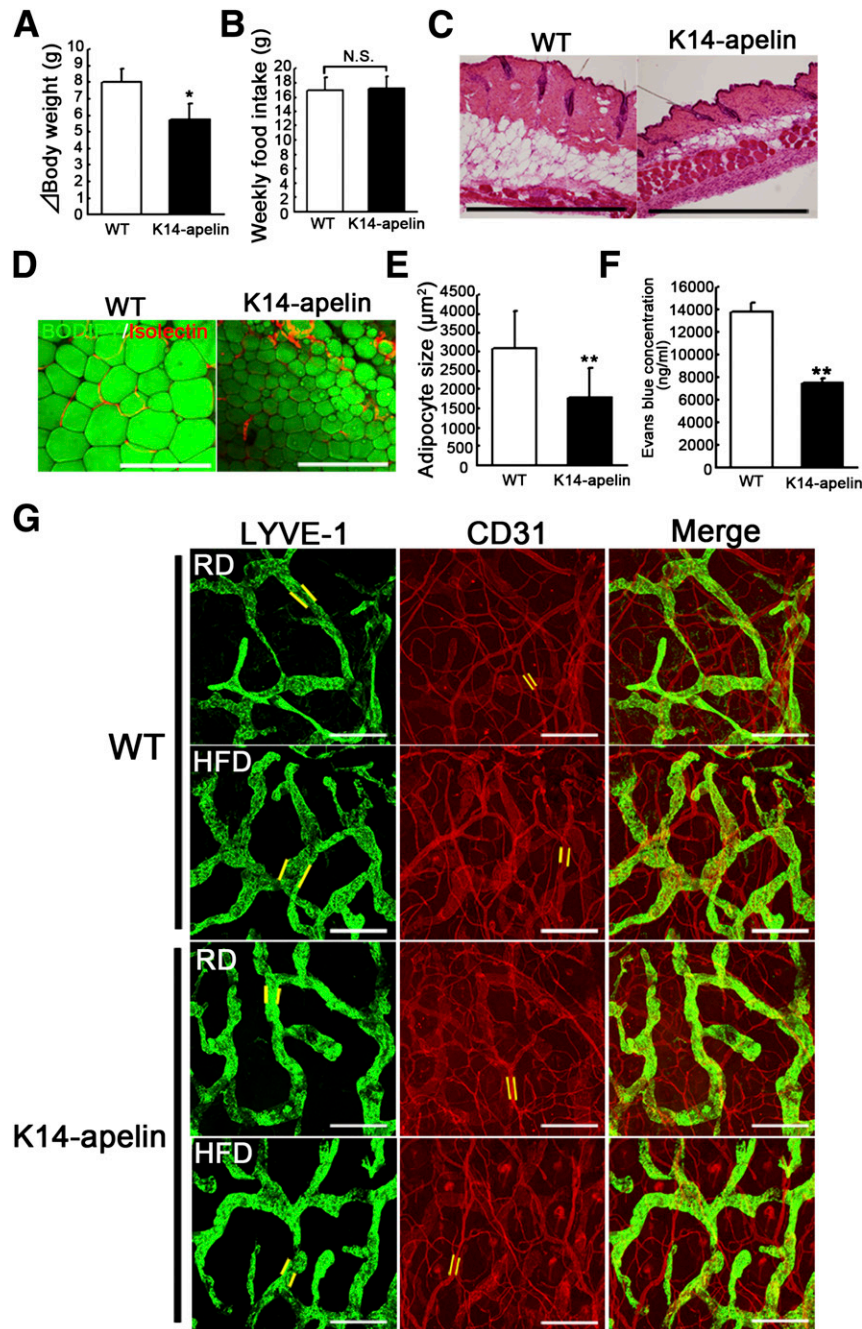
FIG. 6. Resistance to obesity in K14-apelin mice. *A*: Change in body weight of HFD-fed K14-apelin and WT mice (*N* = 4–7). *B*: Average weekly food intake of each genotype. *C*: Hematoxylin and eosin staining of skin sections from HFD-fed, K14-apelin, and WT mice. A reduced subcutaneous adipose layer was found in K14-apelin mice. *D*: BODIPY (green) and Isolectin (red) staining revealed decreased size of subcutaneous adipocytes (green) in K14-apelin mice after HFD feeding. *E*: Morphometric analysis of adipocyte size confirmed that adipocytes were smaller in HFD-fed K14-apelin mice. Data are expressed as mean values ± SD. *F*: Inhibition of lymphatic dye leakage in mesenteric fat of K14-apelin mice after HFD. *G*: Whole-mount staining of mouse ears using antibodies against LYVE-1 (green) and CD31 (red) revealed that HFD induced enlargement of both lymphatic and blood vessels, whereas no significant difference was found between RD- and HFD-fed K14-apelin mice. Two parallel yellow lines as indicated in (*G*) show vascular size. Bars indicate 1 mm (*C*) and 200 μm (*D, G*). **$P < 0.01$, *$P < 0.05$.

dietary fatty acids increased the expression level of transcription factors associated with adipocyte differentiation, including peroxisome proliferator–activated receptors (25), leakage of dietary fatty acids, possibly from hyperpermeable vessels, could accelerate adipocyte differentiation. In addition, a selective COX2 inhibitor did not affect fat accumulation of WT mice, although the number of blood vessels in skin was decreased. Taking into account the fact that no significant change of COX2 expression was found after apelin treatment in endothelial cells, this is consistent with the idea that a selective COX2 inhibitor could directly block the development of vascular hyperpermeability in HFD-fed apelin KO mice, leading to inhibition of obesity. The increased leakage of fatty acids attributable to the disruption of lymphatic and vascular function could trigger adipocyte hypertrophy. Recently, it has been reported that overexpression of COX2 in skin increased energy expenditure via recruitment of brown
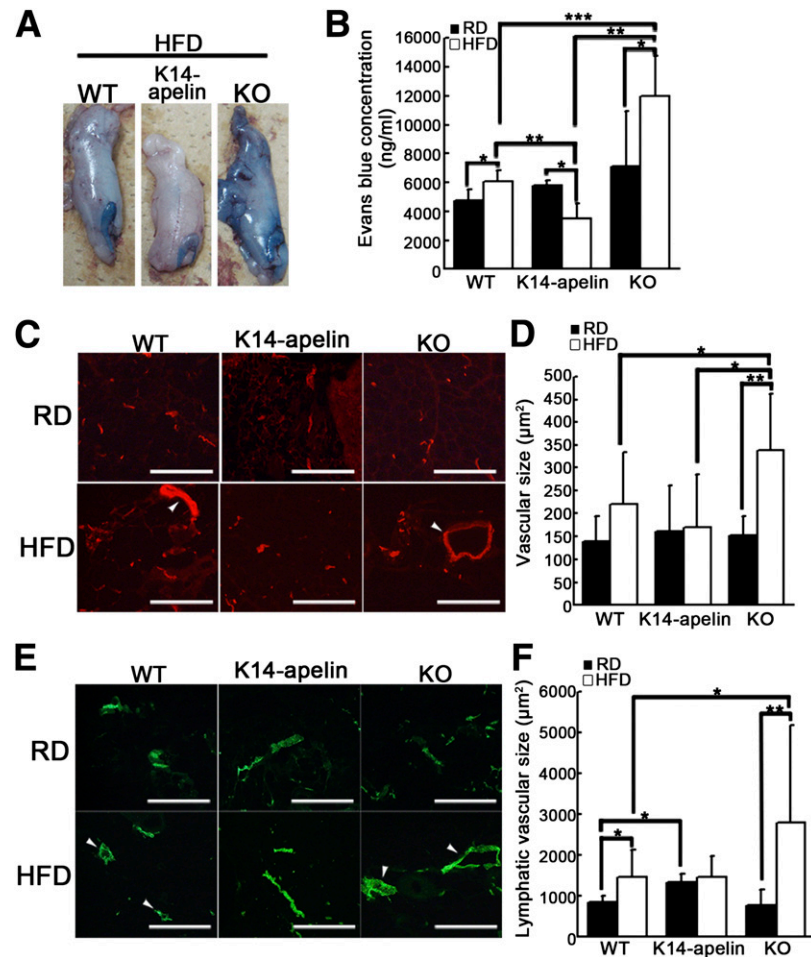
FIG. 7. Structural and functional changes of vessels in the adipose tissues of K14-apelin and apelin KO mice after HFD. A: Miles assay revealed increased Evans blue leakage in epididymal fat of apelin KO mice and decreased leakage in that of K14-apelin mice as compared with WT mice after feeding of HFD. B: Quantitative analysis of dye leakage in the epididymal fat showed that HFD enhanced dye leakage in WT and apelin KO mice, whereas dye leakage was blocked in K14-apelin mice. Immunofluorescence analysis using antibodies against meca-32 (C) and LYVE-1 (E) in mesenteric fat. Arrowheads show enlarged blood vessels (C) and lymphatic vessels (E). Quantitative analysis of blood vessels (D) and lymphatic vessels (F) in mesenteric fat of WT, K14-apelin, and apelin KO mice. Bars indicate 200 μm. **$P < 0.01$, *$P < 0.05$.

adipocytes (26). Therefore, further investigation of the role of apelin in COX2-overexpressing brown adipose tissue is needed.

In conclusion, our results indicate that apelin/APJ signaling promotes lymphatic and blood vessel integrity and blocks the increase of permeability induced by dietary fatty acids, resulting in inhibition of fat accumulation. Apelin might be a novel target for prevention of obesity and obesity-related diseases via enhancement of vascular integrity.

ACKNOWLEDGMENTS

REFERENCES

1. Rosen ED, Spiegelman BM. Adipocytes as regulators of energy balance and glucose homeostasis. Nature 2006;444:847–853
2. Oliver G, Detmar M. The rediscovery of the lymphatic system: old and new insights into the development and biological function of the lymphatic vasculature. Genes Dev 2002;16:773–783
3. Hu FB, Willett WC, Li T, Stampfer MJ, Colditz GA, Manson JE. Adiposity as compared with physical activity in predicting mortality among women. N Engl J Med 2004;351:2694–2703
4. Crandall DL, Hausman GJ, Kral JG. A review of the microcirculation of adipose tissue: anatomic, metabolic, and angiogenic perspectives. Microcirculation 1997;4:211–232
5. Cao Y. Adipose tissue angiogenesis as a therapeutic target for obesity and metabolic diseases. Nat Rev Drug Discov 2010;9:107–115
6. Karkkainen MJ, Saaristo A, Jussila L, et al. A model for gene therapy of human hereditary lymphedema. Proc Natl Acad Sci USA 2001;98:12677–12682
7. Harvey NL, Srinivasan RS, Dillard ME, et al. Lymphatic vascular defects promoted by Prox1 haploinsufficiency cause adult-onset obesity. Nat Genet 2005;37:1072–1081
8. Tatemoto K, Hosoya M, Habata Y, et al. Isolation and characterization of a novel endogenous peptide ligand for the human APJ receptor. Biochem Biophys Res Commun 1998;251:471–476
9. Chen MM, Ashley EA, Deng DX, et al. Novel role for the potent endogenous inotrope apelin in human cardiac dysfunction. Circulation 2003;108:1432–1439
10. Kidoya H, Ueno M, Yamada Y, et al. Spatial and temporal role of the apelin/APJ system in the caliber size regulation of blood vessels during angiogenesis. EMBO J 2008;27:522–534

11. Kidoya H, Naito H, Takakura N. Apelin induces enlarged and nonleaky blood vessels for functional recovery from ischemia. Blood 2010;115:3166–3174

12. Sawane M, Kidoya H, Muramatsu F, Takakura N, Kajiya K. Apelin attenuates UVB-induced edema and inflammation by promoting vessel function. Am J Pathol 2011;179:2691–2697

13. Kajiya K, Hirakawa S, Ma B, Drinnenberg I, Detmar M. Hepatocyte growth factor promotes lymphatic vessel formation and function. EMBO J 2005;24:2885–2895

14. Nishimura S, Manabe I, Nagasaki M, et al. In vivo imaging in mice reveals local cell dynamics and inflammation in obese adipose tissue. J Clin Invest 2008;118:710–721

15. Hirakawa S, Hong YK, Harvey N, et al. Identification of vascular lineage-specific genes by transcriptional profiling of isolated blood vascular and lymphatic endothelial cells. Am J Pathol 2003;162:575–586

16. Yamamoto Y, Yoshimasa Y, Koh M, et al. Constitutively active mitogen-activated protein kinase kinase increases GLUT1 expression and recruits both GLUT1 and GLUT4 at the cell surface in 3T3-L1 adipocytes. Diabetes 2000;49:332–339

17. Calkhoven CF, Müller C, Leutz A. Translational control of C/EBPalpha and C/EBPbeta isoform expression. Genes Dev 2000;14:1920–1932

18. Reaux A, De Mota N, Skultetyova I, et al. Physiological role of a novel neuropeptide, apelin, and its receptor in the rat brain. J Neurochem 2001;77:1085–1096

19. Iwata C, Kano MR, Komuro A, et al. Inhibition of cyclooxygenase-2 suppresses lymph node metastasis via reduction of lymphangiogenesis. Cancer Res 2007;67:10181–10189

20. Mäkinen T, Jussila L, Veikkola T, et al. Inhibition of lymphangiogenesis with resulting lymphedema in transgenic mice expressing soluble VEGF receptor-3. Nat Med 2001;7:199–205

21. Lim HY, Rutkowski JM, Helft J, et al. Hypercholesterolemic mice exhibit lymphatic vessel dysfunction and degeneration. Am J Pathol 2009;175:1328–1337

22. Kajiya K, Hirakawa S, Detmar M. Vascular endothelial growth factor-A mediates ultraviolet B-induced impairment of lymphatic vessel function. Am J Pathol 2006;169:1496–1503

23. Huggenberger R, Ullmann S, Proulx ST, Pytowski B, Alitalo K, Detmar M. Stimulation of lymphangiogenesis via VEGFR-3 inhibits chronic skin inflammation. J Exp Med 2010;207:2255–2269

24. Kajiya K, Sawane M, Huggenberger R, Detmar M. Activation of the VEGFR-3 pathway by VEGF-C attenuates UVB-induced edema formation and skin inflammation by promoting lymphangiogenesis. J Invest Dermatol 2009;129:1292–1298

25. Madsen L, Petersen RK, Kristiansen K. Regulation of adipocyte differentiation and function by polyunsaturated fatty acids. Biochim Biophys Acta 2005;1740:266–286

26. Vegiopoulos A, Müller-Decker K, Strzoda D, et al. Cyclooxygenase-2 controls energy homeostasis in mice by de novo recruitment of brown adipocytes. Science 2010;328:1158–1161